Mechanism of multimodal substrate translocation in P-glycoprotein

Theresa Gewering[1,3]†, Deepali Waghray[2]†, Kristian Parey[1,3], Joel Zapata[5], Pengyi Zhao[6], Hao Chen[6], Dovile Januliene[1,3,4], Ina L. Urbatsch[5], Arne Moeller[1,3,4]*‡, Qinghai Zhang[2]*‡

[1]Osnabrück University, Department of Biology/Chemistry, Structural Biology section, 49076 Osnabrück, Germany.

[2]Department of Integrative Structural and Computational Biology, The Scripps Research Institute, La Jolla, CA 92037, USA.

[3]Department of Structural Biology, Max Planck Institute of Biophysics, 60438 Frankfurt am Main, Germany.

[4]Osnabrück University, Center of Cellular Nanoanalytic Osnabrück (CellNanOs), 49076 Osnabrück, Germany

[5]Department of Cell Biology and Biochemistry, Texas Tech University Health Sciences Center, Lubbock, TX 79430, USA.

[6]Department of Chemistry & Environmental Science, New Jersey Institute of Technology, Newark, New Jersey 07102, USA.

*Corresponding author. Email: arne.moeller@uos.de (A.M.); qinghai@scripps.edu (Q.Z.)

† These authors contributed equally to this work.

‡These authors contributed equally to this work.

Abstract

P-glycoprotein (Pgp) is a highly dynamic ATP-binding cassette transporter that confers cancer multidrug resistance and mediates the bioavailability and pharmacokinetics of many drugs. Structural and biochemical data have provided insights into the binding of diverse compounds, but how they are translocated through the membrane has remained elusive. The biggest hurdle to address this fundamental question has been isolating and characterizing the short-lived transition states during transport. Here, we covalently attached a cyclopeptide substrate to discrete sites of Pgp. Cryo-EM analyses of inward- and outward-facing conformations enabled tracing of the substrate passage and revealed how a cascade of conformational changes in transmembrane helix 1 drives substrate movement across the membrane bilayer upon ATP binding. Observation of a double substrate-bound outward-facing conformation suggests that Pgp can co-transport two compounds simultaneously.

One-Sentence Summary

Cryo-EM reveals the substrate transport pathway and mechanism of P-glycoprotein from initial binding to release.

Main Text:

P-glycoprotein (Pgp, also known as MDR-1 and ABCB1) is a prominent member of the human ATP-binding cassette (ABC) efflux transporters that removes a large variety of chemically unrelated hydrophobic compounds from cells (*1*). Pgp is highly expressed in the liver, kidney, and intestines, where it limits absorption and enhances the excretion of cytotoxic compounds. In the blood-brain, blood-testis, and blood-placenta barriers, Pgp protects and detoxifies those sanctuaries from xenobiotics. Of central importance for many chemotherapeutic treatments, Pgp is a major determinant of drug bioavailability and pharmacokinetics and confers multidrug resistance in several diseases, most notably cancer (*2-4*). Consequently, evasion, selective inhibition, and modulation of Pgp transport are important goals in drug development but are hindered by a lack of detailed understanding of the drug transport mechanisms (*5*).

For Pgp and ABC transporters in general, ATP binding, hydrolysis, and subsequent release of the cleaved products (inorganic phosphate and ADP) fuel large-scale conformational changes that ultimately result in translocation of substrates across the membrane bilayer (*6, 7*). In inward-facing (IF) conformations, the nucleotide-binding domains (NBDs) are separated, and substrates can access a large binding cavity that is open to the lower membrane leaflet and cytoplasm. ATP-induced dimerization of the NBDs promotes large rearrangements of the transmembrane domains (TMDs) between an IF and outward-facing (OF) conformation, from which the substrate is released (*8*). Pgp structures with bound substrates and inhibitors in IF conformation have revealed one or more overlapping binding sites (*9-13*), and multimodal binding mechanisms for chemically related compounds have been proposed (*1, 9*). However, structural data that elucidate how substrates are shuttled through the lipid bilayer are unavailable at present. So far, only a single OF structure of Pgp has been described, but without detectable substrate density (*14*). Most insights

into the transport pathway arise from molecular dynamics simulations, which are also limited by the scarcity of available structural details (*15-17*). Consequently, the molecular mechanics that move the substrate through the transmembrane passage have remained elusive. To address this fundamental question and overcome the dynamic and transient nature of substrate translocation, we developed a novel approach of tethering substrate molecules covalently to specific residues along the putative translocation pathway of Pgp and utilized cryo-EM to capture Pgp structures with bound substrate during various stages of transport.

To take advantage of the highly selective cysteine (Cys) conjugation chemistry, we synthesized a derivative of the previously published QZ-Ala tripeptide substrate (*10*), by substituting one of the three Ala with Cys that is disulfide-linked to a 2,4-dinitrophenyl thiolate group (designated AAC-DNPT, Supplemental methods, fig. S1). DNPT strongly activates disulfide exchange, allowing rapid and efficient crosslinking between the cyclopeptide and accessible cysteines. Free DNPT, released during crosslinking, is bright yellow, providing a simple, visible readout that can be monitored with a UV-Vis spectrometer (Fig. 1A). Three single-Cys mutants of Pgp (Pgp335, Pgp978 and Pgp971) were generated for crosslinking and mutations were chosen near the two QZ-Ala binding sites, known from a previous structure (*10*). L335C in transmembrane helix 6 (TM6) and V978C in TM12 are situated at symmetric positions on opposing TMD halves, while L971C is located two helical turns above V978 (Fig. 1B). Based on the appearance of the yellow DNPT byproduct, Pgp335 and Pgp978 was shown to react with AAC-DNPT within minutes, while Pgp971 did not, with only background absorbance similar to Cys-less Pgp (CL-Pgp) (Fig. 1C). Only after adding Mg^{2+}ATP to fuel substrate translocation could Pgp971 react with AAC-DNPT. Covalent attachment of the AAC-cyclopeptide was further validated by high-resolution mass spectrometry of trypsin-digested peptide fragments (figs. S2 to S4). While QZ-Ala (*10*) and AAC-

DNPT strongly stimulate ATP hydrolysis in CL-Pgp (Fig. 1D), the rate of ATP hydrolysis is reduced after cross-linking. Importantly, Pgp335 and Pgp978 retain notably higher ATPase activity after cross-linking than Pgp971 or the respective apo-Pgp mutants (fig. S5 and Fig. 1D), suggesting that AAC-labeled Pgp335 and Pgp978 still cycle between IF and OF conformations, albeit more slowly.

To capture these different conformations during the transport cycle of Pgp, we mutated the catalytic glutamate residues in the Walker-B motifs of each NBD (E552Q/E1197Q) in Pgp335 and Pgp978. When Mg^{2+}ATP is present, these mutations arrest the enzyme in an ATP-occluded, stabilized NBD dimer conformation that resembles the pre-hydrolysis state (*14*). For Pgp971, we prepared the covalent complex in the presence of Mg^{2+}ATP without introducing the double E/Q mutations as shown in Fig 1C. To stabilize the resulting OF complex, vanadate was included to trap Pgp in a post-hydrolysis intermediate state (*18, 19*). Cryo-EM analysis of the respective covalent complexes in both OF and IF conformations provided eight high-resolution structures with zero, one or two ligands bound (Fig. 2, figs. S6 and S7, and table S1).

An IF-structure of Pgp335, solved at 3.2Å resolution, showed clear densities for two substrate molecules: one crosslinked and one not (IF335-2lig, Figs. 2 and 3). The non-crosslinked molecule, is bound in a position that resembles the one previously reported in a crystal structure (*10*), where it interacts closely with the covalently-linked substrate, which is situated further up the membrane. Both ligand molecules are oriented along the vertical axis of the protein and positioned side-by-side through hydrophobic interactions. The uncleaved DNPT group of the non-crosslinked substrate is evident in the cryo-EM density map. Two substrate molecules are also bound in the IF structure of Pgp978 (IF978-2lig). Despite the lower resolution, limiting the assignment of the

DNPT moiety, the non-covalently bound molecule is clearly visible at the similar position as in IF335-2lig, while the crosslinked substrate is located on the opposite side of the binding cavity (fig. S8). Corroborating our labeling data (Fig. 1C), in the IF structure of Pgp971 (IF971-1lig) at 4.3 Å resolution, only the non-crosslinked substrate is bound at the approximate location seen for non-crosslinked substrate in IF335-2lig and IF978-2lig (Figs. 2 and 3), indicating that the substrate must be transported to residue L971C for the crosslinking reaction to take place.

Multi-model cryo-EM analyses of ATP-bound Pgp335 revealed three different OF conformations within a single dataset: ligand-free (42%), single ligand molecule bound (34%), and double-ligand-bound (26%) (OF335-nolig, OF335-1lig and OF335-2lig), at 2.6 Å, 2.6 Å, and 3.1 Å resolutions, respectively (fig. S9, Supplemental methods). Interestingly, for the Pgp978 and Pgp971, only OF conformations with a single bound ligand (OF978-1lig and OF971-1lig, Fig. 2) were detected at 2.9 Å and 3 Å, respectively.

In the OF structures, the central transmembrane helices TM1, TM6, TM7 and TM12 bulge outwards slightly to accommodate the substrate in a small tunnel, which is collapsed in the ligand-free state (fig. S10). Comparing the ligand positions between the IF and OF structures, in IF335-2lig to OF335-1lig, and IF978-2lig to OF978-1lig, the covalently attached ligand pivots around the respective Cys residue by almost 180°, moving it further up the translocation tunnel (Fig. 3, fig. S8A,B, and movie S1). Our data do not reveal whether rotation of the ligand during the IF-OF conformational change is required for transport or if this reflects the fact that the ligand is covalently pinned to the crosslinking residue. However, the observation of ligand rotation illustrates how much space is available in the binding cavity during this conformational transition. Note that such a reorientation, “flipping” of the substrate, would enable transport of hydrophobic

compounds, such as lipids, and their incorporation into the outer leaflet (*20, 21*). The ligand position and orientation in OF335-1lig and OF978-1lig overall coincide well, with the latter shifting up slightly. This finding indicates that the export tunnel is inherent to the substrate translocation regardless of its initial binding position in the IF conformation (fig. S8D). As such, our data suggest a single common pathway for substrate export in Pgp, contrary to the dual pseudosymmetric pathways suggested earlier (*16, 22*).

The OF971-1lig captures a later-stage transport intermediate, in which the compound resides approximately 7 Å further up the translocation tunnel and is coordinated by highly conserved residues, including M74 and F78 (Figs. 2 and 3). Methionines and phenylalanines at different positions seem to be important for ligand coordination in all of the Pgp structures (fig. S11). As expected, the substrate is held in the binding pocket mainly by the hydrophobic interactions throughout the different conformations (Fig. 3 and fig. S11). Finally, the substrate is released from the OF structure, as represented by OF335-nolig (*14*).

The series of IF and OF Pgp structures reveal a fascinating cascade of conformational changes in TM1, which displays significant plasticity throughout the different transport stages (Figs. 2, 3, and movie S1). In IF conformations, TM1 is a long, straight helix (Figs. 2 and 3). However, in OF335-1lig, OF978-1lig, and OF971-1lig, TM1 swings out at A63, dilating the transmembrane passage and providing sufficient space for accommodating the bound ligand. At the same time, a kink at G72 on TM1 destabilizes the helix and the extracellular loop of Pgp between TM1 and TM2 and leads to a partial unwinding of the helix. This conformational deformation shields the intramembranous tunnel from the extracellular environment, with TM1 acting as a lid, almost parallel to the membrane. Strikingly, along with the upward movement of the ligand (from L335C

to V978C to L971C), the TM1 loop is progressively lifted, restabilized, and ultimately restraightened upon the release of the ligand from the tunnel in the OF335-nolig structure (Fig. 3 and movie S1). Interestingly, the extracellular gate is sealed in all OF structures (fig. S10), which is especially surprising for OF971-1lig where the ligand is near the tunnel exit. To determine whether this conformational change of TM1 loop is itself sufficient to seal the extracellular gate, we removed it computationally, and the calculated diameter of the resulting channel supported our notion (fig. S10).

While superposition of the single ligand-bound OF Pgp structures revealed striking conformational changes in TM1, the double ligand-bound OF conformation in OF335-2lig displays marked differences. Here, all of the transmembrane helices undergo significant conformational changes inflating the center of the tunnel and generating space for two substrates (fig. S12), while TM1 does not show the characteristic kinking described above (Fig. 3). In this case, TM12 displays the most pronounced reorientation moving away from the center while the top of the extracellular gate remains fully closed (fig. S10). The bound substrates are rotated approximately by 90° with respect to the position of single ligand in OF335-1lig (fig. S8C). Unexpectedly, the crosslinked substrate in OF335-2lig sits below its initial position in the IF conformation, with the non-crosslinked molecule situated above (fig. S8C). The fact that the non-crosslinked molecule remains in the translocation tunnel suggests that its release is blocked by the crosslinked ligand. We cannot determine if the ligand would be released from this state without crosslinking, but the observation of this dual ligand-bound OF conformation indicates that Pgp may be able to co-transport two substrate molecules in one catalytic cycle.

Our data suggest a mechanism for how Pgp mediates substrate transport (Fig. 4, and movie S1). Transport commences in the IF conformation with binding of one or two substrate molecules. Upon ATP-induced NBD-dimerization, the transporter converges into an OF conformation in which the intracellular gate is closed. The presence of the substrate in the OF conformation of Pgp dislocates TM1 at A63 and introduces a sharp kink at G72, forcing the helix into an energetically unfavorable conformation. Simultaneously, the distal section of TM1 unfolds, conserving the energy from NBD dimerization. These structural changes result in an enlarged extracellular loop that shields the transmembrane tunnel from the extracellular environment. The intrinsic propensity of TM1 to return to an energetically favorable state pushes the substrate up the translocation tunnel, allowing TM1 to gradually restabilize. During the last stages of transport (OF971-1lig to OF335-nolig), the TM1-TM2 regulatory loop straightens, and the substrate-interacting hydrophobic residues (M74 and F78) rotate and pivot away from the tunnel. The rotations of these residues suggest that the substrate is pulled out into the extracellular space by a corkscrew-like mechanism. Note that, although OF971-1lig captured a post-hydrolysis state, we cannot rule out the possibility of ligand release prior to ATP hydrolysis, were this not precluded by covalent binding. Notwithstanding, the proposed TM1 kinking and straightening mechanism of substrate expulsion would, therefore, obviate the requirement for the Y-shaped, wide-open OF conformation, reported for multiple other ABC transporters (*23, 24*), suggesting a substrate-dependent transport mechanism in Pgp, or else a divergence of mechanisms among ABC transporters.

How ABC transporters move substrates through the lipid bilayer has been a long-standing question (*25*). The scarcity of high-resolution structures of substrate-bound OF conformations (*26*), especially in the highly transient intermediate states, has severely limited our understanding of this vital process. Here, we were able to determine eight high-resolution structures of the archetypical

ABC transporter Pgp, revealing the underlying molecular mechanics of substrate translocation. In general, the large number and diversity of ABC transporters, and the even wider variety of their substrates, make it unlikely that a universal substrate translocation mechanism will emerge. Our strategy of stalling the otherwise highly transient intermediates in this process through crosslinking and subsequent high-resolution cryo-EM analysis could serve as a blueprint to understand the transport mechanisms of lipid transporters as well as other members of the transporter family.

References and Notes

1. E. E. Chufan, H. M. Sim, S. V. Ambudkar, Molecular basis of the polyspecificity of P-glycoprotein (ABCB1): recent biochemical and structural studies. *Adv. Cancer Res.* **125**, 71-96 (2015).
2. K. M. Giacomini *et al.*, Membrane transporters in drug development. *Nat. Rev. Drug Discov.* **9**, 215-236 (2010).
3. M. M. Gottesman, V. Ling, The molecular basis of multidrug resistance in cancer: the early years of P-glycoprotein research. *FEBS Lett.* **580**, 998-1009 (2006).
4. R. W. Robey *et al.*, Revisiting the role of ABC transporters in multidrug-resistant cancer. *Nat. Rev.. Cancer* **18**, 452-464 (2018).
5. D. Waghray, Q. Zhang, Inhibit or evade multidrug resistance P-glycoprotein in cancer treatment. *J. Med. Chem.* **61**, 5108-5121 (2018).
6. D. C. Rees, E. Johnson, O. Lewinson, ABC transporters: the power to change. *Nat. Rev. Mol. Cell Biol.* **10**, 218-227 (2009).
7. S. Hofmann *et al.*, Conformation space of a heterodimeric ABC exporter under turnover conditions. *Nature* **571**, 580-583 (2019).
8. D. Januliene, A. Moeller, Cryo-EM of ABC transporters: an ice-cold solution to everything? *FEBS Lett.* **594**, 3776-3789 (2020).
9. S. G. Aller *et al.*, Structure of P-glycoprotein reveals a molecular basis for poly-specific drug binding. *Science* **323**, 1718-1722 (2009).
10. P. Szewczyk *et al.*, Snapshots of ligand entry, malleable binding and induced helical movement in P-glycoprotein. *Acta Crystallogr. Section D, Biol. Crystallog.* **71**, 732-741 (2015).
11. A. Alam *et al.*, Structure of a zosuquidar and UIC2-bound human-mouse chimeric ABCB1. *Proc. Natl. Acad. Sci. U. S. A.* **115**, E1973-E1982 (2018).
12. A. Alam, J. Kowal, E. Broude, I. Roninson, K. P. Locher, Structural insight into substrate and inhibitor discrimination by human P-glycoprotein. *Science* **363**, 753-756 (2019).
13. K. Nosol *et al.*, Cryo-EM structures reveal distinct mechanisms of inhibition of the human multidrug transporter ABCB1. *Proc. Natl. Acad. Sci. U. S. A.* **117**, 26245-26253 (2020).
14. Y. Kim, J. Chen, Molecular structure of human P-glycoprotein in the ATP-bound, outward-facing conformation. *Science* **359**, 915-919 (2018).
15. H. Goddeke, L. V. Schafer, Capturing substrate translocation in an ABC exporter at the atomic level. *J. Am. Chem. Soc.* **142**, 12791-12801 (2020).
16. J. W. McCormick, P. D. Vogel, J. G. Wise, Multiple drug transport pathways through human P-Glycoprotein. *Biochemistry* **54**, 4374-4390 (2015).
17. B. Verhalen *et al.*, Energy transduction and alternating access of the mammalian ABC transporter P-glycoprotein. *Nature* **543**, 738-741 (2017).
18. I. L. Urbatsch, B. Sankaran, S. Bhagat, A. E. Senior, Both P-glycoprotein nucleotide-binding sites are catalytically active. *J. Biol. Chem.* **270**, 26956-26961 (1995).
19. A. Moeller *et al.*, Distinct conformational spectrum of homologous multidrug ABC transporters. *Structure* **23**, 450-460 (2015).
20. A. van Helvoort *et al.*, MDR1 P-glycoprotein is a lipid translocase of broad specificity, while MDR3 P-glycoprotein specifically translocates phosphatidylcholine. *Cell* **87**, 507-517 (1996).
21. Y. Romsicki, F. J. Sharom, Phospholipid flippase activity of the reconstituted P-glycoprotein multidrug transporter. *Biochemistry* **40**, 6937-6947 (2001).

22. Z. Parveen *et al.*, Molecular dissection of dual pseudosymmetric solute translocation pathways in human P-glycoprotein. *Mol. Pharmacol.* **79**, 443-452 (2011).
23. A. Ward, C. L. Reyes, J. Yu, C. B. Roth, G. Chang, Flexibility in the ABC transporter MsbA: Alternating access with a twist. *Proc. Natl. Acad. Sci. U. S. A.* **104**, 19005-19010 (2007).
24. R. J. Dawson, K. P. Locher, Structure of a bacterial multidrug ABC transporter. *Nature* **443**, 180-185 (2006).
25. C. Fan, J. T. Kaiser, D. C. Rees, A structural framework for unidirectional transport by a bacterial ABC exporter. *Proc. Natl. Acad. Sci. U. S. A.* **117**, 19228-19236 (2020).
26. V. Chaptal *et al.*, Substrate-bound and substrate-free outward-facing structures of a multidrug ABC exporter. *Sci. Adv.* **8**, eabg9215 (2022).
27. D. J. Swartz *et al.*, Directed evolution of P-glycoprotein cysteines reveals site-specific, non-conservative substitutions that preserve multidrug resistance. *Biosci. Rep.* **34**, 297-310 (2014).
28. J. Bai *et al.*, A gene optimization strategy that enhances production of fully functional P-glycoprotein in *Pichia pastoris*. *PloS One* **6**, e22577 (2011).
29. M. E. Zoghbi *et al.*, Substrate-induced conformational changes in the nucleotide-binding domains of lipid bilayer-associated P-glycoprotein during ATP hydrolysis. *J. Biol. Chem.* **292**, 20412-20424 (2017).
30. I. L. Urbatsch, B. Sankaran, J. Weber, A. E. Senior, P-glycoprotein is stably inhibited by vanadate-induced trapping of nucleotide at a single catalytic site. *J. Biol. Chem.* **270**, 19383-19390 (1995).
31. I. L. Urbatsch, G. A. Tyndall, G. Tombline, A. E. Senior, P-glycoprotein catalytic mechanism: studies of the ADP-vanadate inhibited state. *J. Biol. Chem.* **278**, 23171-23179 (2003).
32. T. Gewering, D. Januliene, A. B. Ries, A. Moeller, Know your detergents: A case study on detergent background in negative stain electron microscopy. *J. Struct. Biol.* **203**, 242-246 (2018).
33. D. Januliene, A. Moeller, Single-Particle Cryo-EM of Membrane Proteins. *Methods Mol. Biol.* **2302**, 153-178 (2021).
34. A. Punjani, J. L. Rubinstein, D. J. Fleet, M. A. Brubaker, cryoSPARC: algorithms for rapid unsupervised cryo-EM structure determination. *Nat. Methods* **14**, 290-296 (2017).
35. S. H. Scheres, RELION: implementation of a Bayesian approach to cryo-EM structure determination. *J. Struct. Biol.* **180**, 519-530 (2012).
36. A. Punjani, H. Zhang, D. J. Fleet, Non-uniform refinement: adaptive regularization improves single-particle cryo-EM reconstruction. *Nat. Methods* **17**, 1214-1221 (2020).
37. J. L. Rubinstein, M. A. Brubaker, Alignment of cryo-EM movies of individual particles by optimization of image translations. *J. Struct. Biol.* **192**, 188-195 (2015).
38. T. Bepler, K. Kelley, A. J. Noble, B. Berger, Topaz-Denoise: general deep denoising models for cryoEM and cryoET. *Nat. Commun.* **11**, 5208 (2020).
39. T. C. Terwilliger, S. J. Ludtke, R. J. Read, P. D. Adams, P. V. Afonine, Improvement of cryo-EM maps by density modification. *Nat. Methods* **17**, 923-927 (2020).
40. P. Emsley, K. Cowtan, Coot: model-building tools for molecular graphics. *Acta Crystallogr. D, Biol. Crystallogr.* **60**, 2126-2132 (2004).
41. P. V. Afonine *et al.*, Real-space refinement in PHENIX for cryo-EM and crystallography. *Acta Crystallogr. D Struct. Biol.* **74**, 531-544 (2018).
42. V. B. Chen *et al.*, MolProbity: all-atom structure validation for macromolecular crystallography. *Acta Crystallogr. D, Biol. Crystallogr.* **66**, 12-21 (2010).

43. T. D. Goddard *et al.*, UCSF ChimeraX: Meeting modern challenges in visualization and analysis. *Protein Sci.* **27**, 14-25 (2018).
44. E. Chovancova *et al.*, CAVER 3.0: a tool for the analysis of transport pathways in dynamic protein structures. *PLoS Comput. Biol.* **8**, e1002708 (2012).
45. A. C. Wallace, R. A. Laskowski, J. M. Thornton, LIGPLOT: a program to generate schematic diagrams of protein-ligand interactions. *Protein Eng.* **8**, 127-134 (1995).
46. K. Katoh, H. Toh, Parallelization of the MAFFT multiple sequence alignment program. *Bioinformatics* **26**, 1899-1900 (2010).
47. X. Robert, P. Gouet, Deciphering key features in protein structures with the new ENDscript server. *Nucleic Acids Res.* **42**, W320-324 (2014).

Acknowledgments: We thank J.-H. Leung, W.-H. Lee, and A. Ward for early contributions, C. Katz for technical assistance, S. Welsh, S. Prinz and W. Kühlbrandt for generous access to the cryo-EM facilities in Frankfurt and general support, and W. Kühlbrandt and I. Wilson for critical reading and editing of the manuscript. **Funding:** This work was supported by National Institute of General Medical Sciences R01 GM118594 (Q.Z.), the Deutsche Forschungsgemeinschaft (DFG) Sonderforschungsbereich 944 (A.M.), the Max Planck Society (A.M. & T.G.), the Boehringer Ingelheim Fonds (T.G.) and the South Plains Foundation (I.L.U.). **Author contributions:** TG performed cryo-EM and single particle analysis with help from DJ and AM. DW conducted ligand synthesis and crosslinking, identified Pgp single Cys mutants, performed biochemical characterization, and optimized and prepared Pgp samples for mass spectrometry and cryo-EM studies under the supervision of QZ. PZ performed mass spectrometric characterization of crosslinking under the supervision of HC. KP built molecular models with help from TG and AM. JZ expressed Pgp mutants under the supervision of ILU. QZ and ILU conceived the Pgp labeling experiments and designed and tested the mutations. AM designed and supervised the cryo-EM research. AM, TG and DJ interpreted the cryo-EM structural data with significant input from QZ. QZ conceived and initiated the project, designed the research, and coordinated collaborations. The manuscript was written by TG, DW, DJ, ILU, QZ and AM. All authors carefully discussed and interpreted the data. **Competing interests:** Authors declare that they have no competing interests. **Data and materials availability:** All cryo-EM density maps have been deposited in the Electron Microscopy Data Bank under accession numbers EMD-14754, EMD-14755, EMD-14756, EMD-14757, EMD-14758, EMD-14759, EMD-14760 and EMD-14761. Atomic coordinates for the atomic models have been deposited in the Protein Data Bank under accession numbers 7ZK4, 7ZK5, 7ZK6, 7ZK7, 7ZK8, 7ZK9, 7ZKA and 7ZKB. All other data are available in the main text or supplementary materials.

Fig. 1. Covalent ligand design for Pgp transport studies. (**A**) Design of AAC-DNPT, a derivative of QZ-Ala cyclopeptide, for disulfide crosslinking with single-cysteine mutants of Pgp; yellow product DNPT used as readout. (B) Positions of L335 (TM6), V978 and L971 (TM12) in Pgp, residues targeted for cyclopeptide labeling. (C) Monitoring covalent reaction between AAC-DNPT and cysteine mutants (+/- Mg^{2+}ATP) by UV-visible spectrometry; CL-Pgp was used as a control. (**D**) ATPase activities of L335C, V978C, and L971C before and after crosslinking with AAC-DNPT; CL-Pgp was used as a control.

Fig. 2. High-resolution structures of Pgp with bound ligands. For all mutants, IF and OF structures were obtained. For Pgp335 three different OF conformations were detected in one data set (OF335-nolig, OF335-1lig, OF335-2lig). To display the binding sites the upper halves of TM 2,10,11 and 12 were removed from the densities. For the IF structures, TM9 was also removed for clarity. TM1 is shown in brown, with the covalently bound ligand in red and the non-crosslinked in grey**.** A zoom-in of TM1 in the black box region is shown in Fig. 3.

Fig. 3. Close-up on TM1 in all Pgp structures. The crosslinked ligand (AAC) is shown in red, the non-crosslinked one (AAC-DNPT) in grey. Residues A63 and G72 are indicated in green as the breaking points in TM1, and the interacting residues M68, M74 and F78 in pink. The crosslinked residue is shown in cyan.

Fig. 4. Mechanism of Pgp ligand transport. Pgp binds the ligand in the IF state. ATP binding induces dimerization of NBDs and converts Pgp to OF conformation. TM1 (brown) kinks to make space for the ligand (red) in the binding cavity of OF Pgp. TM1 gradually restraightens and restabilizes, while it pushes the ligand up the exit tunnel. After ligand release, TM1 reverts to a straight helix.

Fig. 1.

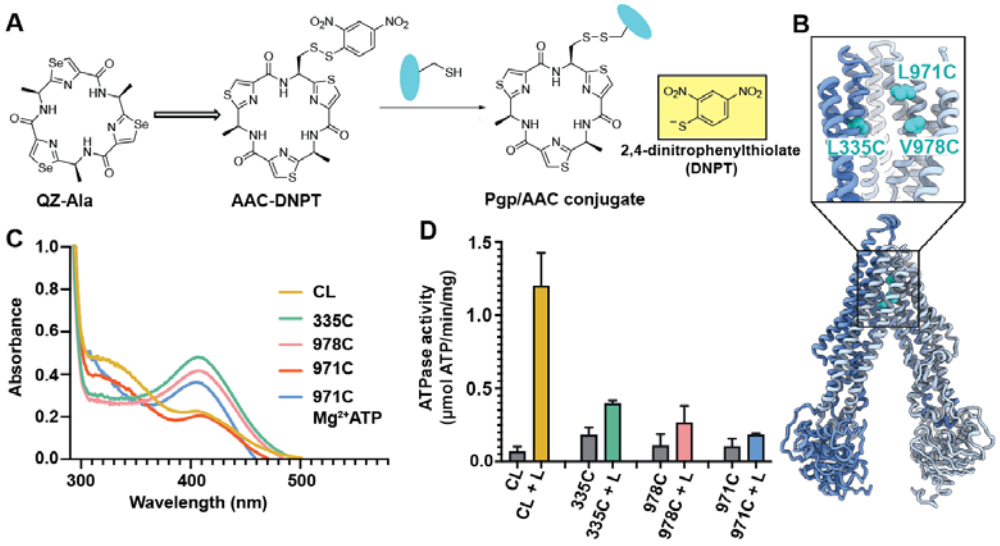
A
QZ-Ala
AAC-DNPT
Pgp/AAC conjugate
2,4-dinitrophenylthiolate
(DNPT)
B
L971C
L335C
V978C
C
Absorbance
Wavelength (nm)
CL
335C
978C
971C
971C
Mg²⁺ATP
D
ATPase activity
(µmol ATP/min/mg)
CL
CL + L
335C
335C + L
978C
978C + L
971C
971C + L

Fig. 2.

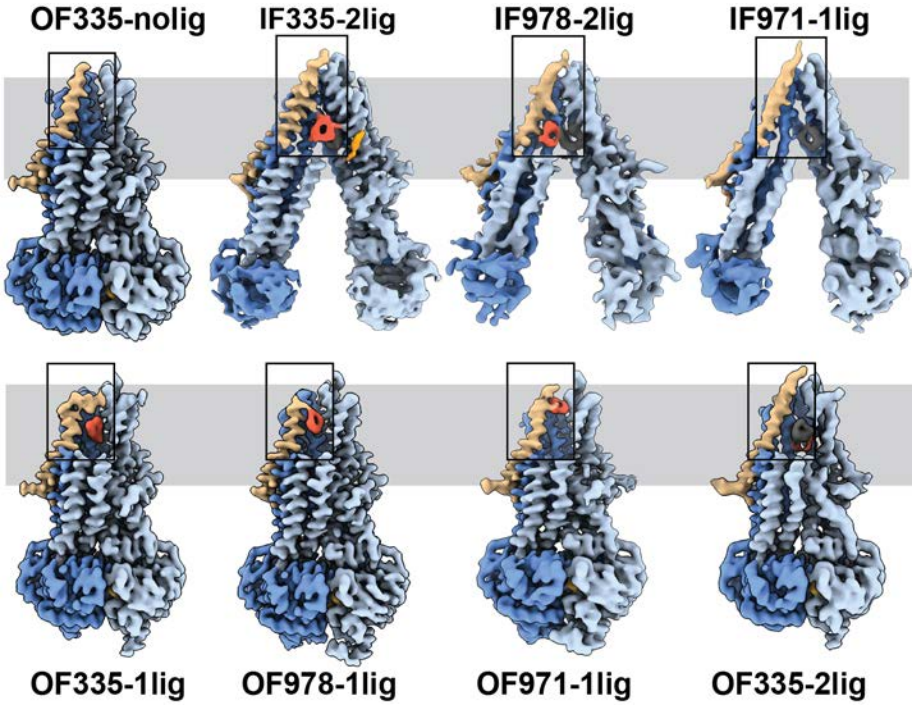
OF335-nolig
IF335-2lig
IF978-2lig
IF971-1lig
OF335-1lig
OF978-1lig
OF971-1lig
OF335-2lig

Fig. 3.

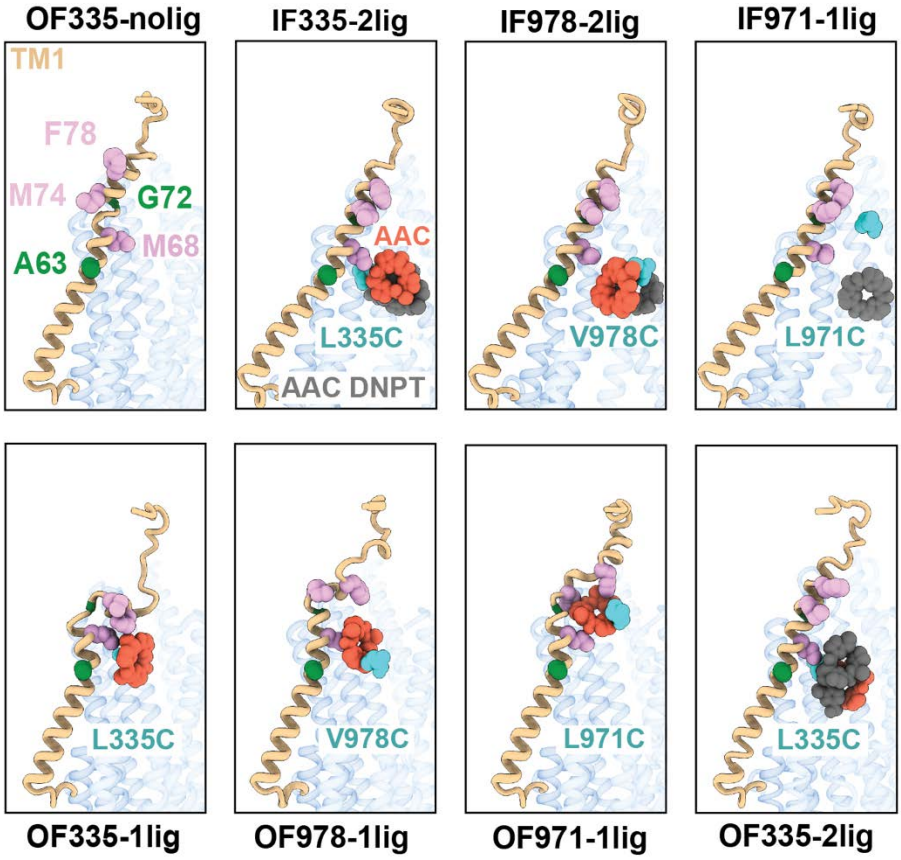
OF335-nolig
IF335-2lig
IF978-2lig
IF971-1lig
TM1
F78
M74
G72
M68
A63
AAC
L335C
AAC DNPT
V978C
L971C
L335C
V978C
L971C
L335C
OF335-1lig
OF978-1lig
OF971-1lig
OF335-2lig
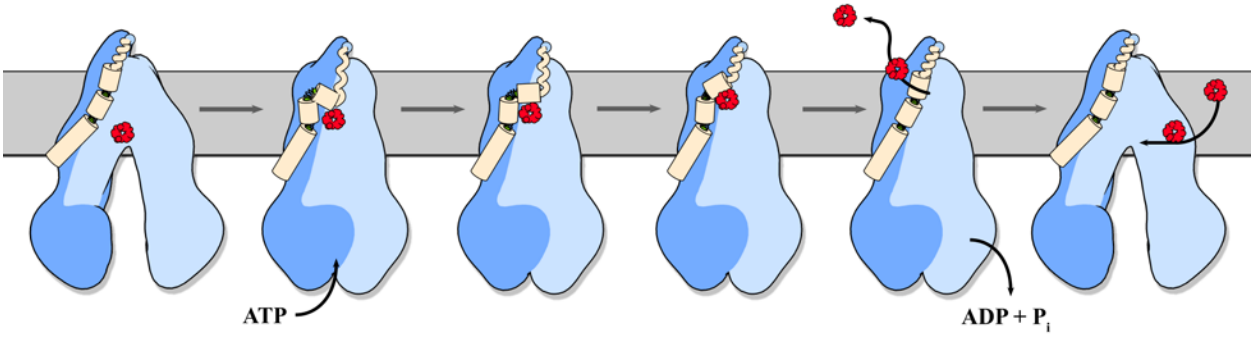
Fig. 4.